Computational Materials Science 97 (2015) 102–108

Contents lists available at ScienceDirect

Computational Materials Science

journal homepage: www.elsevier.com/locate/commatsci

Effect of Re on lattice trapping in γ′-Ni_3Al cracks by atomistic simulation

Shu-Lan Liu [a], Chong-Yu Wang [a,b,*], Tao Yu [a], Zheng-Guang Liu [a,c]

[a] Central Iron and Steel Research Institute, Beijing 100081, China
[b] Department of Physics, Tsinghua University, Beijing 100084, China
[c] Department of Physics, North University of China, Taiyuan 030051, China

ARTICLE INFO

Article history:
Received 29 April 2014
Received in revised form 29 September 2014
Accepted 7 October 2014

Keywords:
Lattice trapping
γ′-Ni_3Al
Crack
Re
Molecular dynamics

ABSTRACT

The effect of Re on the lattice trapping at three different crack orientations in γ′-Ni_3Al was studied using the molecular dynamics (MD) method with a Ni–Al–Re embedded-atom-method (EAM) potential. The simulation results showed that the lattice trapping limits ($K_{IC}^{\pm}$) were not influenced by a single Re atom, while they were influenced by additions of 3 at.% or 6 at.% Re atoms. The calculation values of $K_{IC}^{\pm}$ increased with the increasing of Re concentration. This revealed that the strength of γ′-Ni_3Al can be effectively improved by Re addition, which was in agreement with previous studies. Furthermore, the lattice trapping ranges (ΔK) were small (never exceeded 4% of the theoretical Griffith load K_{th}^{G}) for all the crack systems with or without Re. At different crack orientations for the crack systems with the same Re concentration, there were different lattice trapping limits. Moreover, there were bendings of atomic rows near the Re atoms. This is due to the bonding strength of Ni–Re is stronger than that of Ni–Al, which was confirmed by the discrete-variational method (DVM) calculation.

1. Introduction

Final rupture in materials is displayed by the fracture of atomic bond at crack tip. From an atomic point of view, the rupture manifests as the discreteness of lattice rather than the fracture of homogeneous continuum. The discrete atomic bond, relating with the lattice resistance to crack advance, causes the crack to remain stable and not to advance or heal within a certain load range, until the loads somewhat larger or smaller than the Griffith load (K_{th}^{G}) are reached. The phenomenon was called lattice trapping effect, which was first described by Thomson et al. [1]. The critical loads for a crack to advance or heal are called the upper and lower lattice trapping limits ($K_{IC}^{\pm}$), respectively. The K_{IC}^{+} can be identified at which the activation energy barrier (AEB) against bond breaking vanishes and bond breaks spontaneously without the aid of thermal activation; similarly, the K_{IC}^{-} can be identified at which the AEB against bond healing vanishes [2–4]. In general, the lattice trapping limits are closely related to the fracture stress. Therefore, there is a need to study the lattice trapping of a crack to investigate the fracture in material.

It was reported that there are many factors that can affect the lattice trapping, such as the crack front direction, crack propagation direction and interatomic potential [2,5,6]. Zhang et al. [3] indicated that the lattice trapping strength depends on the interaction range of the interatomic force fields, and the lattice trapping effect is caused by the lattice discreteness and independent of crack length. Schoeck and Pichl [7] showed that the lattice trapping range mainly depends on the relative stiffness of the crack-tip bond as compared to the combined stiffness of all the bonds that load the crack-tip atoms. Further investigations [3,8,9] pointed out that for a close-packed lattice and "soft" interatomic interaction model (e.g. the crack propagation in Ni), and long-range interatomic potentials, the lattice trapping effect is small. However, when doping Re in Ni matrix phase, the lattice trapping limits can be increased significantly due to the stronger interatomic interaction of Ni–Re [10].

The main structure of Ni-based single crystal (SC) superalloys is the ordered γ′-Ni_3Al precipitation phase with $L1_2$ structure, which is coherently embedded in a matrix of the γ-Ni phase [11,12]. The deformation behavior of γ′-Ni_3Al can partially reflect the mechanical properties of Ni-based superalloys. At present, some experimental researches [13,14] about crack propagation in γ′-Ni_3Al were reported. Re is a critical element for the remarkable improvement of mechanical properties of superalloys [15–19]. While, the strengthening mechanism of Ni-based SC superalloys due to the addition of Re is not fully understood. It was proved that Re mainly partitions into the γ′ phase in ternary alloy [20,21]; and a certain number of Re atoms partition into the γ′ phase in multi-component superalloys [22–24]. At present, the strengthening mechanism of

* Corresponding author at: Department of Physics, Tsinghua University, Beijing 100084, China. Tel.: +86 01062772782.
E-mail addresses: shulan070@126.com (S.-L. Liu), cywang@mail.tsinghua.edu.cn (C.-Y. Wang), ytao012345@163.com (T. Yu), guang212@163.com (Z.-G. Liu).

http://dx.doi.org/10.1016/j.commatsci.2014.10.011
0927-0256/

Re doped in γ′-Ni_3Al was properly investigated by the first-principles approach [25–28]. However, the mechanisms of fracture and strength in superalloys are complex, and brittle fracture may also exist in superalloys, which in turn may restrict the use of high-temperature structural materials. The previous works were mainly focused on the analysis of electronic structures, which are not sufficient to fully understand the strengthening mechanism of γ′-Ni_3Al with Re addition. Therefore, there is a need to investigate the influence of Re on fracture in γ′-Ni_3Al on the atomic level. It was well known that the crack in superalloys often propagates in a ductile manner at high temperature and in a cleavage manner at low temperature. In order to compare the molecular dynamics (MD) simulation result with that of the first-principles calculation, herein the temperature 0 K was adopted to perform the simulation.

In the present study, the effect of Re on the lattice trapping at the (010)[001], (101)[010] and (010)[101] crack orientations in γ′-Ni_3Al was investigated at 0 K, using the MD simulation with a Ni–Al–Re EAM potential [29] and the XMD program [30]. The contents to be discussed included the influences of a single Re atom at the crack tip and different Re concentrations (3 at.% or 6 at.% Re atoms randomly distributed in the γ′-Ni_3Al phase) on the lattice trapping of a crack. It needs to be mentioned that, the Re concentration (3 at.% or 6 at.%) is larger than the experimental value, but it will not influence our purpose of this study. Our concern was mainly focused on comparing the simulation results of the two concentrations with that of 0 Re, to study the trend of the effect of different Re concentrations on lattice trapping.

2. Conditions of computer simulation

2.1. Model of crack

In the present study, three different crack orientations of mode I cracks were chosen, including the (010)[001], (101)[010] and (010)[101] crack orientations (as shown in Table 1). Herein the (010) and (101) indicate the directions of the crack planes; the [001], [010] and [101] indicate the directions of the crack front. For instance, the (010)[001] crack system was shown in Fig. 1. For each crack orientation, three different Re concentrations (0 Re, 3 at.% and 6 at.% Re atoms) in Ni_3Al were considered. The dimensions of all the crack systems are shown in Table 1. As an example, at the (010)[001] crack orientation, there are 80 atomic layers along the x[100] direction, 100 atomic layers along the y[010] direction and 160 atomic layers along the z[001] direction, containing 640,000 atoms in total. For the systems with 0 Re, 3 at.% and 6 at.% Re atoms addition, the lattice constants of the relaxed systems are 3.567 Å, 3.571 Å and 3.576 Å, respectively. The reason that the lattice constants increase with Re addition can be explained by the larger Re atomic radius (1.37 Å). Moreover, a larger simulation box (in which the dimension of z direction is 2 times larger than that in Table 1) at each crack orientation was tested, and it was found that the basic results, such as the average binding energy, surface energy and lattice trapping limits, were insensitive to the change in the system size. Thus, the smaller simulation sizes (as shown in Table 1) were considered to perform the simulation. The crack was constructed according to the anisotropic linear elastic continuum mechanics equations [31] with a desired stress intensity factor K_I. And the initial crack length was about l_o = 45 Å. The periodic boundary condition was applied in the direction parallel to the crack front, while the fixed-displacement boundary conditions (the outer four atomic layers were fixed) were applied in the directions of crack plane and crack propagation. A time step of 5×10^{-15} s was used. The Ni–Al–Re embedded-atom-method (EAM) potential [29], which can successfully describe the effect of Re in the Ni–Al crack system [10,32], has been applied.

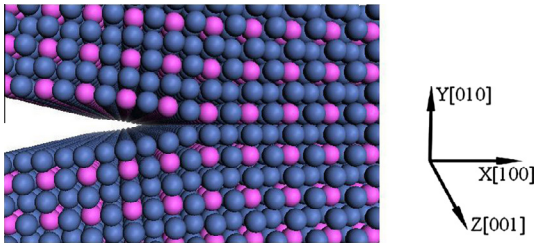

Fig. 1. Side view of the atomic configuration for the (010)[001] crack tip.

In order to estimate the site preference behavior of Re in Ni_3Al, the average binding energy for the perfect system with (or without) Re was calculated using the MD method, and the simulation box at the (010)[001] crack orientation as shown in Table 1 is used to perform the simulation. The calculated results for the systems with 0 Re, 3 at.% and 6 at.% Re atoms randomly doped to the Ni or Al sites are summarized in Table 2. The lower value of the average binding energy indicates that Re atom prefers to occupy the corresponding site. Apparently, it can be seen from Table 2 that Re atom preferentially occupies the Al site, which is in agreement with the previous theoretical and experimental studies [21,25,33,34]. Thus, Re atoms substitutes for Al sites in all the doped systems in the present study. In addition, for Ni_3Al, the difference of the average binding energy between the present study (−4.65 eV) and the previous result (−4.63 eV) [35] is negligible, which also reveals that the Ni–Al–Re EAM potential is reliable for the present study.

2.2. Evaluation criteria of lattice trapping limits

The cracks were initially configured at different loads, and then the atoms at crack tip were fully relaxed with the boundary

Table 1
Dimensions, atomic number and surface energy (γ) for the three types of crack systems (including the (010)[001], (101)[010] and (010)[101] crack orientations). Each type of crack system contains the three different Re concentrations (0 Re, 3 at.% and 6 at.% Re) in γ′-Ni_3Al.

Crack orientation	Dimensions	System	Number of atoms (Ni + Al + Re)	γ (J/m^2)
(010)[001]	$\frac{80}{2} \times \frac{100}{2} \times \frac{160}{2} a^3$	0 Re	480,000 + 160,000 + 0	1.795
		3 at.% Re	480,000 + 140,800 + 19,200	1.799
		6 at.% Re	480,000 + 121,600 + 38,400	1.802
(101)[010]	$\frac{120}{4}\sqrt{2} \times \frac{120}{4}\sqrt{2} \times \frac{160}{2} a^3$	0 Re	432,000 + 144,000 + 0	1.883
		3 at.% Re	432,000 + 126,720 + 17,280	1.892
		6 at.% Re	432,000 + 109,440 + 34,560	1.900
(010)[101]	$\frac{120}{4}\sqrt{2} \times \frac{80}{2} \times \frac{240}{4}\sqrt{2} a^3$	0 Re	432,000 + 144,000 + 0	1.795
		3 at.% Re	432,000 + 126,720 + 17,280	1.799
		6 at.% Re	432,000 + 109,440 + 34,560	1.801

Note: "a" indicates the lattice constant of the relaxed system.

Table 2
Average binding energy (E_{eatom}) for the perfect Ni_3Al system at the (010)[001] crack orientation, with or without Re addition. "Re–Ni" or "Re–Al" indicates that Re substitutes for Ni or Al in Ni_3Al, respectively.

System	Ni_3Al		Re–Ni		Re–Al	
	Previous[a]	This work	3 at.% Re	6 at.% Re	3 at.% Re	6 at.% Re
E_{eatom} (eV/atom)	−4.63	−4.65	−4.74	−4.84	−4.76	4.88

[a] [38].

conditions mentioned above. The scheme of loading or unloading has been described in the literatures [6,10] which was started at a stress intensity that fulfilled the Griffith criterion (crack tip structures are stable at the load, namely the crack tip does not advance or heal). Then, the relaxed structures were taken as the starting points for further loading or unloading by proportional scaling of the boundary displacements. The increment of loading or unloading was 1% of the Griffith load. According to the sudden increase and decrease of the average bond lengths at the crack tip, the upper and lower trapping limits ($K_{IC}^{\pm}$) were determined, respectively [6,36].

The average bond length at the crack tip is expressed as follows [10]:

$$d_{ij} = \frac{1}{m}\sum_{k=1}^{m} l_{ijk}, \tag{1}$$

where d_{ij} is the average bond length of atom pairs between atomic row i (in the lower crack surface) and atomic row j (in the upper crack surface), and m is the total atomic number in atomic row i or j. l_{ijk} is the bond length of the atom pair k (which is consisted of the atom from row i of the lower crack surface and the corresponding atom from row j of the upper crack surface). As an example, Fig. 2 shows the atomic configurations of the ten atomic rows (i, j = 1, 2, 3, 4, 5) at the (010)[001] crack tip. There are five average bond lengths (d_{11}, d_{22}, d_{33}, d_{44}, d_{55}) between the ten atomic rows at the crack orientation. Herein, the structure of the crack tip is stable when the bond length was in the range of 2.65–4.22 Å, and when the bond length was more than 4.22 Å the crack tip was taken as advancing (in the present study, the value of 4.22 Å is consistent with the value of crack formation length, which was obtained by fitting the relation between the decohesion energy and the opening distance [37]).

After evaluating the upper and lower lattice trapping limits ($K_{IC}^{\pm}$), the lattice trapping range (ΔK) can be obtained from [6]

$$\Delta K = K_{IC}^{+}/K_{IC}^{-} - 1. \tag{2}$$

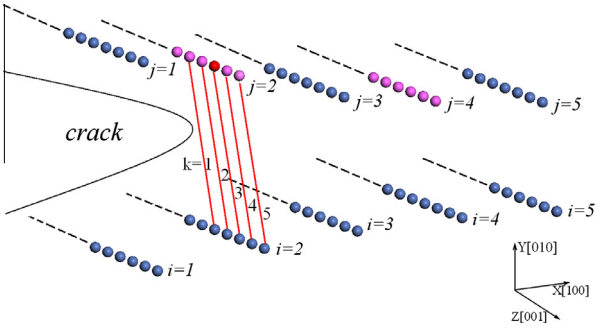

Fig. 2. Atomic configurations of ten atomic rows (i, j = 1, 2, 3, 4, 5) at the (010)[001] crack tip, with a single Re atom at the crack front. The blue, pink and red balls represent Ni, Al and Re atoms, respectively. The red solid lines represent the bond lengths (l_{221}, l_{222}, l_{223}, l_{224}, and l_{225}) of five corresponding atom pairs (k = 1, 2, 3, 4, 5) between the atomic rows i = 2 and j = 2. (For interpretation of the references to color in this figure legend, the reader is referred to the web version of this article.)

In order to explore the influence of Re on the lattice trapping of a crack, two doping schemes were adopted. One is that a single Re atom was placed at the crack front, to probe the influence of Re in the dilute Ni_3Al (Re) solid solution; the other is that 3 at.% or 6 at.% Re atoms were randomly doped into the entire crack system, to probe the influence of Re in the concentrated Ni_3Al (Re) solid solution.

3. Results and discussion

3.1. Influence of a single Re atom on lattice trapping of crack

A single Re atom is placed at the crack front at each crack orientation to study its effect on the lattice trapping of crack. As shown in Fig. 2, the red atom is the single Re atom at the (010)[001] crack tip. Fig. 3 gives the variations in the five average bond lengths at the (010)[001] crack tip with the loading stress intensity factor, without or with a single Re atom at the crack front. From the relation of bond length with K_I/K_{th}^G in Fig. 3(a), we can find that there are slight jumps in the average bond lengths between $K_I/K_{th}^G = 1.01$ and 1.02. Namely, when $K_I/K_{th}^G > 1.01$, the bond lengths clearly increase and the crack tips advance. Therefore, it can be determined that the upper trapping limit for the system without Re at the (010)[001] crack orientation is $K_{IC}^{+} = 1.01K_{th}^G$. Comparing Fig. 3(a) with Fig. 3(b), it is noticed that the jumps in the bond lengths for the system with a single Re atom at the crack front also occur between $K_I/K_{th}^G = 1.01$ and $K_I/K_{th}^G = 1.02$. This means that the calculation value of K_{IC}^{+} is not affected by a single Re atom. Moreover, as shown in Fig. 3(b), the bond breaking of Ni–Re is simultaneous with the others (Ni–Al) along the crack front when $K_I/K_{th}^G = 1.02$ is reached.

Fig. 4 shows the variations in the average bond lengths with the unloading stress intensity factor at the (010)[001] crack tip, without (Fig. 4(a)) or with (Fig. 4(b)) a single Re atom at the crack front. It can be found from Fig. 4 that there are both slight jumps of the curves in the range of $K_I/K_{th}^G = 1.00—0.99$ in the two graphs. Namely, when $K_I/K_{th}^G < 1.00$, the average bond lengths decrease and the crack tips begin to heal. So we can say that the lower trapping limit is $K_{IC}^{-} = 1.00K_{th}^G$, whether or not with a single Re atom at the crack front. This suggests that a single Re atom has no influence on the K_{IC}^{-}.

What is more, as shown in Figs. 3 and 4, the bond breaking or healing of the several consecutive atomic rows at the crack tip take place simultaneously. And this case is the same with that of a single Re atom in Ni [10]. This may be related to the long-range character of interatomic interactions in metal materials. Thus, the breaking or healing of atomic bonds in Ni_3Al should be determined based on the observations of several consecutive atomic rows at the crack tip. The calculation values of $K_{IC}^{\pm}$, for the systems with and without a single Re atom at the crack front, are listed in Table 3. The results in Table 3 show that a single Re atom does not affect $K_{IC}^{\pm}$ and ΔK of the entire crack system. The other three different positions of a single Re atom at the crack front were also considered. The tested results show that the lattice trapping limits and range as well as the bond breaking or healing are not influenced by the different positions of the Re substitution at the crack tip.

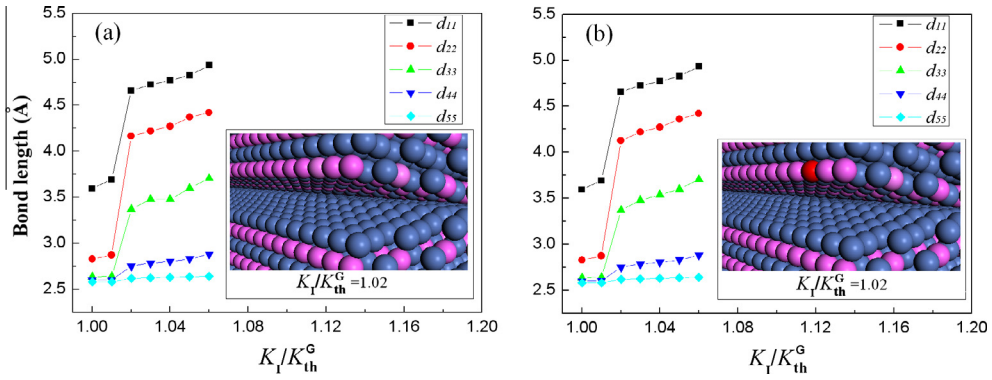

Fig. 3. Variations of the five average bond lengths (including d_{11}, d_{22}, d_{33}, d_{44}, d_{55}) at the (010)[001] crack tip with the loading stress intensity factor and atomic configurations of the crack tip at $K_I/K^G_{th} = 1.02$: (a) without a single Re atom at the crack front and (b) with a single Re atom at the crack front. The blue, pink and red balls represent Ni, Al and Re atoms, respectively. (For interpretation of the references to color in this figure legend, the reader is referred to the web version of this article.)

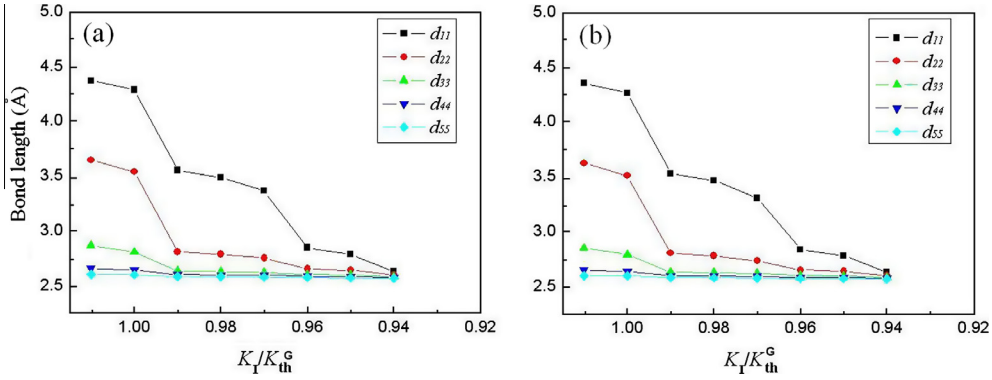

Fig. 4. Variations of the five average bond lengths (including d_{11}, d_{22}, d_{33}, d_{44}, d_{55}) at the (010)[001] crack tip with the unloading stress intensity factor: (a) without a single Re atom at the crack front and (b) with a single Re atom at the crack front.

Besides, there are no kink pairs and atomic rearrangement near the single Re atom along the crack front in the dilute Ni_3Al(Re) solid solutions, for all the types of crack systems. But before the breaking of the atomic bonds, there is slight bending of atomic row (as shown in Fig. 5(a) or $K_I/K^G_{th} = 0.99 \sim 1.01$ in Fig. 6(a)) along the direction perpendicular to the crack propagation at the crack front during the loading process. The bending of atomic row appears near the single Re atom (in the upper crack surface) and the two Ni atoms (in the lower crack surface). This means the interatomic interaction of Ni–Re is stronger than that of Ni–Al, which will be discussed in Section 3.3. Combining with the results in Table 3, it can be found that the lattice trapping limits are not influenced by the bending of atomic row near the single Re atom.

Table 3
Lattice trapping limits ($K^{\pm}_{IC}$) and range (ΔK) for the systems (0 Re, 1 Re, 3 at.% and 6 at.% Re in γ′-Ni_3Al) at the crack orientations of the (010)[001], (101)[010] and (010)[101].

Crack orientation	System	$\frac{K^-_{IC}}{K^G_{th}}$	$\frac{K^+_{IC}}{K^G_{th}}$	ΔK
(010)[001]	0 Re	1.00	1.01	0.010
	1 Re	1.00	1.01	0.010
	3 at.% Re	1.03	1.06	0.029
	6 at.% Re	1.08	1.12	0.037
(101)[010]	0 Re	1.03	1.06	0.029
	1 Re	1.03	1.06	0.029
	3 at.% Re	1.05	1.07	0.019
	6 at.% Re	1.09	1.13	0.037
(010)[101]	0 Re	0.99	1.03	0.040
	1 Re	0.99	1.03	0.040
	3 at.% Re	1.01	1.05	0.040
	6 at.% Re	1.05	1.09	0.038

Note: K^G_{th} is the theoretical Griffith stress intensity factor.

3.2. Influence of Re concentration on lattice trapping of crack

In this section, 3 at.% or 6 at.% Re atoms are randomly doped in γ′-Ni_3Al at each crack orientation to discuss the influence of Re concentration on the lattice trapping of crack.

To confirm the reliability of the random doping and test the influence of different randomness on lattice trapping limits, herein four different random distributions of Re in γ′-Ni_3Al are considered at each crack orientation. For instance, the lattice trapping limits for the crack systems with 3 at.% and 6 at.% Re atoms at the (010)[001] crack orientation are listed in Table 4. It can be found from Table 4 that the errors (which are no more than 0.01) of the lattice trapping limits for the four different distributions are negligible. Therefore, the random doping is reliable for this study. In order to obtain a more accurate result at the (010)[001] crack orientation, the calculation value of K^+_{IC} or K^-_{IC} is the average value of the four tested values (as shown in Table 4). Similarly, the lattice trapping limits at the other two crack orientations are obtained, and the simulation results of $K^{\pm}_{IC}$ and ΔK are also listed in Table 3. It can be seen that the lattice trapping limits ($K^{\pm}_{IC}$) increase with the increasing of Re concentration, for all the crack systems at the three crack orientations. For instance, for the crack systems with 0 Re, 3 at.% and 6 at.% Re atoms at the (010)[001] crack orientation, the values of K^-_{IC}/K^G_{th} are 1.00, 1.03 and 1.08, and that of K^+_{IC}/K^G_{th} are 1.01, 1.06 and 1.12, respectively. This means that the atomic interaction of Ni–Re can promote the healing of crack and prevent the breaking of atomic bonds (namely, prevent the advancing of crack).

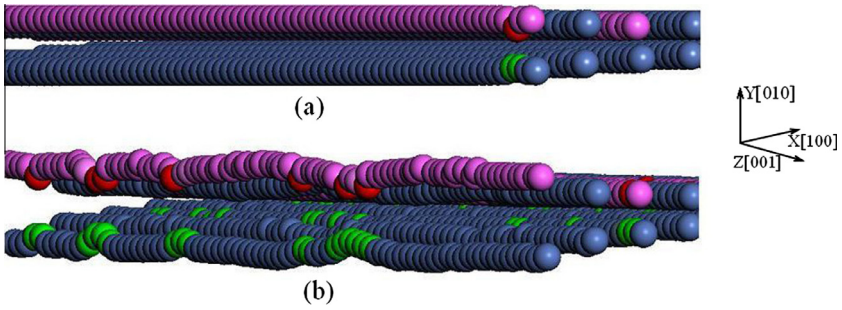

Fig. 5. Atomic configurations of the (010)[001] crack tip: (a) with a single Re atom at the crack front at $K_I/K^G_{th} = 1.00$ and (b) with 3 at.% Re atoms at the crack front at $K_I/K^G_{th} = 1.05$. The blue, pink, red and green balls represent Ni, Al, Re and Ni (near Re atoms in the lower crack surface) atoms, respectively. (For interpretation of the references to color in this figure legend, the reader is referred to the web version of this article.)

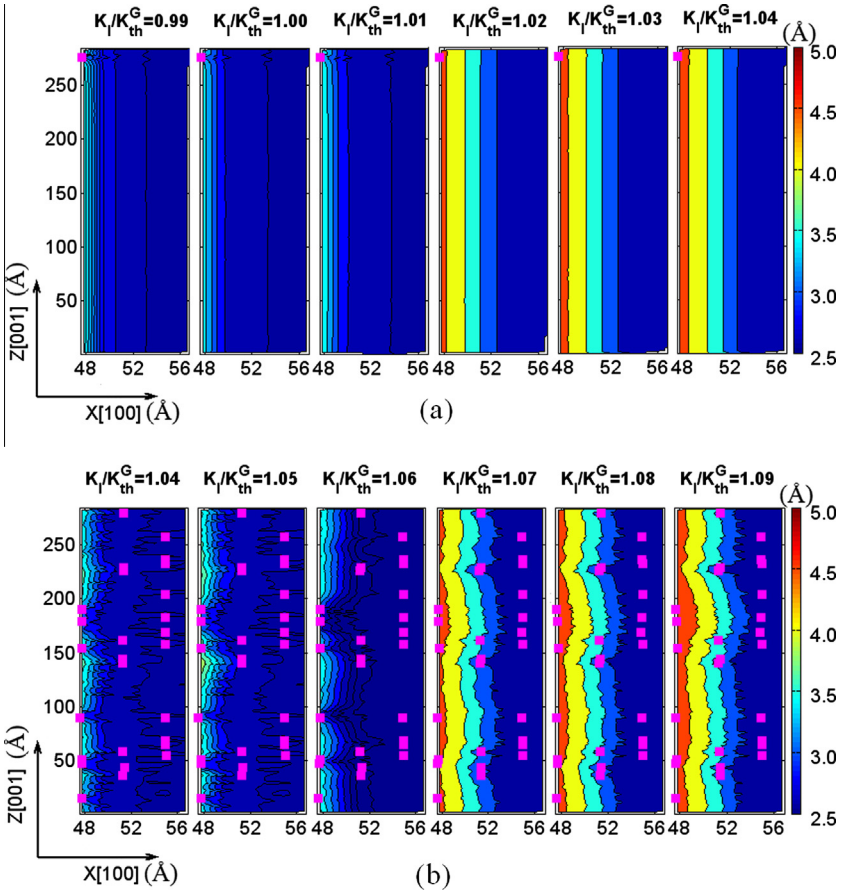

Fig. 6. Contour maps of bond lengths for every atom pair across the (010)[001] crack surface during the loading process: (a) with a single Re atom at the crack front and (b) with the addition of 3 at.% Re atoms. The pink squares represent the positions of the Re atoms, the other different colors represent different bond lengths at the crack tip. (For interpretation of the references to color in this figure legend, the reader is referred to the web version of this article.)

Table 4
Lattice trapping limits ($K^{\pm}_{IC}$) for four different randomness (A, B, C, D) at the (010)[001] crack orientation, for the systems with the addition of 3 at.% or 6 at.% Re atoms.

Randomness	3 at.% Re		6 at.% Re	
	$\frac{K^-_{IC}}{K^G_{th}}$	$\frac{K^+_{IC}}{K^G_{th}}$	$\frac{K^-_{IC}}{K^G_{th}}$	$\frac{K^+_{IC}}{K^G_{th}}$
A	1.03	1.06	1.09	1.12
B	1.03	1.06	1.08	1.12
C	1.02	1.05	1.08	1.12
D	1.03	1.05	1.08	1.12

Note: K^G_{th} is the theoretical Griffith stress intensity factor.

However, the lattice trapping ranges are all small (no more than 4%) at the three crack orientations, even though 3 at.% or 6 at.% Re atoms are doped into the crack systems. This reveals that the long-range interatomic potential and the "soft" interatomic interaction model are used here [9]. It has been pointed out that for the long-range interatomic potential, the lattice trapping of bond breaking at the crack tip is negligible [3].

Comparing the values of $K^{\pm}_{IC}$ in Table 3, it can be seen that for the crack systems with the same Re concentration, the lattice trapping limits are different at the different crack orientations. For instance, the values of K^-_{IC}/K^G_{th} for the systems with 3 at.% Re atoms are 1.03, 1.05 and 1.01, respectively, for the crack orientations of

(010)[001], (101)[010] and (010)[101]. That is because the cleavage fracture of material is directional anisotropic. At different directions of the crack front and crack propagation, the degrees of "easy" and "tough" to crack advance are different [5,6,38]. This indicates that the lattice trapping is related to the directions of crack front and propagation. Another observation is that, whether or not adding Re atoms for the crack systems at the (101)[010] crack orientation, the stability ranges do not include K^G_{th}. Namely, the lower lattice trapping limits are more than $1.00K^G_{th}$. This may be related to the surface energy in different crack systems. According to the Griffith theory for brittle fracture, a plane with the lowest surface energy should be the preferred cleavage plane, and a crack will propagate on this plane. In the present study, we calculate the surface energy (γ), which can be obtained from the following equation [32] $\gamma = \frac{E_{off}-E_{on}}{2A}$, where E_{off} is the potential energy of the model with the periodic boundary condition in the x and z directions, and the free boundary condition in the y direction; E_{on} is the potential energy of the model with the periodic boundary condition in the x, y and z directions; A is the area of the y plane. The results in Table 1 show that the surface energy of the (101) plane is larger than that of the (010) plane for the crack systems, whether or not with the Re atoms. For instance, the surface energy at the (101)[010] crack orientation without Re is 1.883 J/m^2, and the surface energies at the other two orientations are all 1.795 J/m^2. Therefore, the load required for the crack propagation in the (101) plane is larger than that in the (010) plane.

Just as the same with a single Re atom at the crack front, there are no kink pairs during the loading or unloading process, for all the crack systems with 3 at.% or 6 at.% Re atoms. Whereas, as shown in Fig. 5(b), there are bendings of atomic rows near Re atoms along the direction perpendicular to the crack propagation at the crack front. This implies the stronger interaction (cf. Section 3.3) of Re (in the upper crack surface) and Ni atoms (in the lower crack surface). Fig. 6(b) shows the contour maps of bond lengths for every atom pair across the (010)[001] crack surface for the systems with 3 at.% Re atoms during the loading process. The pink squares represent the positions of the Re atoms, and the other different colors represent different bond lengths at the crack tip. As shown at $l = 48$ Å from $K_I/K^G_{th} = 1.04$ to $K_I/K^G_{th} = 1.06$ and at $l = 52$ Å from $K_I/K^G_{th} = 1.07$ to $K_I/K^G_{th} = 1.09$, there are obvious bendings of atomic rows near the Re atoms.

In addition, the lattice trapping limits for the systems at the three crack orientations (as shown in Table 1) are simulated at room temperature (300 K). And the calculated results for the systems (0 Re, 1 Re, 3 at.% or 6 at.% Re atoms in γ'-Ni_3Al) at the (010)[001] crack orientation are listed in Table 5. Comparing the values of $K^{\pm}_{IC}$ simulated at 0 K (as shown in Table 3) and 300 K (as shown in Table 5), it can be seen that at the (010)[001] crack orientation the simulation values of $K^{\pm}_{IC}$ at 300 K are almost the same with that of 0 K. This case is the same with that of the other crack orientations. And there are no dislocations and atomic rearrangements during the process of crack propagation. This reveals that the crack configurations are insensitive to the temperature at 0–300 K.

Table 5
Lattice trapping limits ($K^{\pm}_{IC}$) for the systems (0 Re, 1 Re, 3 at.% or 6 at.% Re in γ'-Ni_3Al) at the (010)[001] crack orientation at 300 K.

System	$\frac{K^-_{IC}}{K^G_{th}}$	$\frac{K^+_{IC}}{K^G_{th}}$
0 Re	1.00	1.01
1 Re	1.00	1.01
3 at.% Re	1.03	1.06
6 at.% Re	1.09	1.13

Note: K^G_{th} is the theoretical Griffith stress intensity factor.

3.3. Bonding strengths of Ni–Re and Ni–Al

From the above discussion, it is known that there are bendings of atomic rows near Re atoms, and Re can affect the lattice trapping limits for the crack systems with 3 at.% or 6 at.% Re atoms in γ'-Ni_3Al. And we attribute the reason to the stronger interatomic interaction of Ni–Re. Thus, it is necessary to compare the bonding strengths of Ni–Re and Ni–Al.

At first, the bonding strength between atoms can be roughly estimated from the well depth of the pair potential in the EAM potential [39], and the interatomic interactions of Ni–Al and Ni–Re in the previous work are shown in Fig. 7. It is noticed that the pole coordinate of the Ni–Al curve is (2.52, −0.31), and that of the Ni–Re curve is (2.65, −0.35). Namely, the absolute value of the potential well depth of the latter (0.35 eV) is larger than that of the former (0.31 eV), and the increasing value is 13%. This indicates that the interatomic interaction of Ni–Re is stronger than that of Ni–Al.

Then, in order to accurately test whether the Re–Ni bond is stronger than the Ni–Al bond in Ni_3Al, we explore the interaction between atoms from the interatomic energy (IE) [25,40] that can be used to evaluate the bonding strength of atoms in a local region, using the ab initio calculation. The IE is defined as

$$E_{lj} = \sum_n N_n \sum_{\alpha\beta} a^*_{n\alpha l} a_{n\beta j} H_{\beta j \alpha l}, \tag{3}$$

where N_n is the electron occupation number for the molecular orbital ψ_n, and $H_{\beta j \alpha l}$ is the Hamiltonian matrix element that connects the atomic orbital β of atom j to the atomic orbital α of atom l. The coefficient $a_{n\alpha l}$ is obtained from $a_{n\alpha l} = \langle \phi_{\alpha l} | \psi_n(r) \rangle$. The IE can be used to evaluate the bonding strengths of two adjacent atoms for it is related to the Hamiltonian matrix element. A larger absolute value of a negative IE means a stronger interatomic interaction. The IE is obtained using the discrete-variational method (DVM), which has been successfully used to describe the electronic structures of metals and alloys [41,42].

In the calculation of the IE, at first, two models (with and without a single Re atom, respectively) are constructed. Each of them consists of 4000 atoms, with 20 atomic layers along the x[100], y[010] and z[001] directions, respectively. The Re (in the model with a single Re atom) atom occupies the Al site at the center of the model. Then, each model is relaxed by the MD simulation with the Ni–Al–Re EAM potential. Finally, a cluster (as shown in Fig. 8) containing 171 atoms which locate at the center of the MD model is selected out to perform the DVM calculation. Fig. 8(a) and (b) are the configurations with and without a Re atom (the blue, pink and red balls represent Ni, Al and Re atoms), respectively. The green balls are Ni atoms which are the nearest-neighbor atoms of Re12

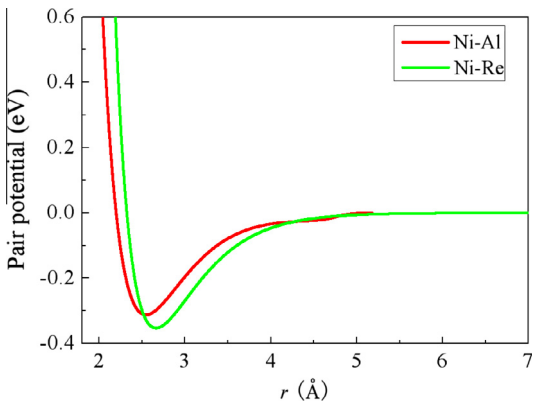

Fig. 7. Variations of pair potential with the distance of Ni–Al and Ni–Re atoms.

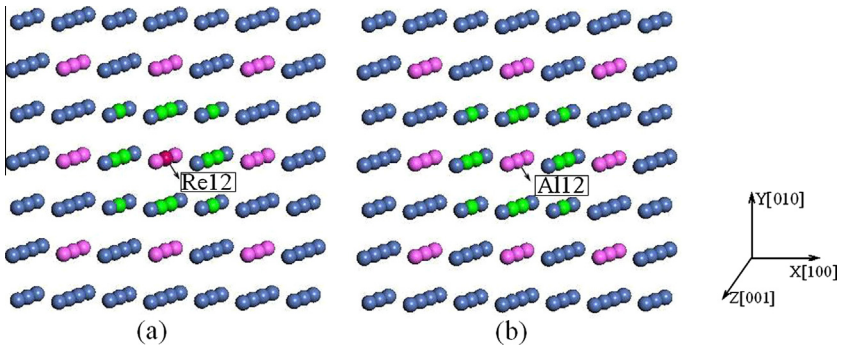

Fig. 8. Configurations of 171 atoms: (a) with a single Re atom and (b) without Re. The blue, pink and red balls represent Ni, Al and Re atoms, respectively. The green balls (Ni atoms) represent the nearest-neighbor atoms of Re12 (or Al12). (For interpretation of the references to color in this figure legend, the reader is referred to the web version of this article.)

(or Al12). More calculation details for the IE can be found in the literatures [40,43]. Here the spin-polarization calculation is performed. We compute the average value of the interatomic energies between Re12 (or Al12) and the 12 nearest-neighbor atoms. The calculation results show that the average value of the IE of Ni–Al is −0.98 eV, and that of Ni–Re is −1.76 eV. Namely, the absolute value of IE increases by 79.6% on addition of Re. This means that the bonding strength of Ni–Re is indeed stronger than that of Ni–Al, which compares well with the previous results [25–28].

It can be concluded that due to the stronger interatomic interaction of Ni–Re, the bendings of atomic rows appear near the Re atoms at the crack front, and Re can promote the crack healing and prevent the bond breaking in γ′-Ni_3Al. The calculation values of $K_{IC}^{\pm}$ increased with the addition of 3 at.% or 6 at.% Re atoms, which reveals that the fracture strength of γ′-Ni_3Al can be improved with Re addition. For metallic materials, the lattice trapping of cracks is difficult to study directly by experiments, due to the fact that metals do not show the larger trapping effects and are not brittle enough [8,10]. However, the effect of Re on the improvement of mechanical strength in superalloys in the present study can be supported by the previous theoretical [25–28] and experimental [17–19] results.

4. Conclusions

In summary, three types of mode I cracks are fabricated to study the effect of Re on the lattice trapping of crack in γ′-Ni_3Al. The simulation results show that a single Re atom does not affect $K_{IC}^{\pm}$. With the addition of 3 at.% or 6 at.% Re atoms in γ′-Ni_3Al, the calculation values of $K_{IC}^{\pm}$ increase with the increasing of Re concentration. This means that the interaction of Ni–Re can promote the healing of crack and prevent the breaking of atomic bonds in γ′-Ni_3Al. Regardless of the addition of Re, the lattice trapping ranges at the three crack orientations are all small. This is related with the long-range interatomic potential. During the loading process, due to the stronger interaction of Ni–Re atomic bond, there are bendings of atomic rows near the Re atoms at the crack front. The effect of Re on the improvement of mechanical properties in superalloys is in agreement with the previous reports. The present study supplies a good theoretical guidance for the brittle fracture of Ni-based superalloys in the future research.

Acknowledgments

We are grateful to Professor L.G. Wang for beneficial discussions. This work was supported by the National Basic Research Program of China (Grant No. 2011CB606402) and the National Natural Science Foundation of China (Grant No. 51071091). The simulations were carried out on the "Explorer 100" cluster system of Tsinghua National Laboratory for Information Science and Technology, Beijing, China.

References

[1] R. Thomson, C. Hsieh, V. Rana, J. Appl. Phys. 42 (1971) 3154–3160.
[2] J.C.H. Spence, Y.M. Huang, O. Sankey, Acta Metall. Mater. 41 (1993) 2815–2824.
[3] S.L. Zhang, T. Zhu, T. Belytschko, Phys. Rev. B 76 (2007) 094114.
[4] T. Zhu, J. Li, S. Yip, Proc. R. Soc. A 462 (2006) 1741–1761.
[5] S. Kohlhoff, P. Gumbsch, H.F. Fischmei, Philos. Mag. A 64 (1991) 851–878.
[6] R. Pérez, P. Gumbsch, Phys. Rev. L 84 (2000) 5347–5350.
[7] G. Schoeck, W. Pichl, Phys. Status Solidi A 118 (1990) 109–115.
[8] P. Gumbsch, R.M. Cannon, MRS Bull. 25 (2000) 15.
[9] P. Gumbsch, J. Mater. Res. 10 (1995) 2897–2907.
[10] Z.G. Liu, C.Y. Wang, T. Yu, Comput. Mater. Sci. 83 (2014) 196–206.
[11] T.M. Pollock, S. Tin, J. Propul. Power 22 (2006) 361–374.
[12] E.A. Loria, Superalloy 718: Metallurgy and Applications, TMS, Warrendale, PA, 1989.
[13] Z.W. Shan, X. Wu, L. Liu, J.H. Yang, Y.B. Xu, Mater. Sci. Technol. 17 (2001) 1398–1402.
[14] M. Dao, B.K. Kad, R.J. Asaro, Philos. Mag. A 75 (1997) 443–459.
[15] G.L. Erickson, The Development and Application of CMSX-10, TMS, Warrendale, PA, 1996, pp. 35–44.
[16] W.S. Walston, K.S. O'Hara, E.W. Ross, T.M. Pollock, W.H. Murphy, RENÉ N6: Third Generation Single Crystal Superalloy, TMS, Warrendale, PA, 1996, pp. 27–34.
[17] A.F. Giamei, D.L. Anton, Metall. Trans. A 16 (1985) 1997–2005.
[18] A.D. Cetel, D.N. Duhl, Second Generation Columnar Grain Nickel-Base Superalloy, TMS, Warrendale, PA, 1992, pp. 287–296.
[19] B.D. Bryskin (Ed.), Rhenium and Rhenium Alloys, TMS, Warrendale, PA, 1997, pp. 731–754.
[20] A. Volek, F. Pyczak, R.F. Singer, H. Mughrabi, Scr. Mater. 52 (2005) 141–145.
[21] X.X. Yu, C.Y. Wang, X.N. Zhang, P. Yan, Z. Zhang, J. Alloys Compd. 582 (2014) 299–304.
[22] Y. Amouyal, D.N. Seidman, Acta Mater. 59 (2011) 3321–3333.
[23] R.C. Reed, A.C. Yeh, S. Tin, S.S. Babu, M.K. Miller, Scr. Mater. 51 (2004) 327–331.
[24] A.C. Yeh, S. Tin, Scr. Mater. 52 (2005) 519–524.
[25] S.Y. Wang, C.Y. Wang, J.H. Sun, W.H. Duan, D.L. Zhao, Phys. Rev. B 65 (2001) 035101.
[26] Y.J. Wang, C.Y. Wang, Philos. Mag. 89 (2009) 2935–2947.
[27] Y.J. Wang, C.Y. Wang, Scr. Mater. 61 (2009) 197–200.
[28] Y.J. Wang, C.Y. Wang, MRS Proc. 1224 (2010). 1224–FF05.
[29] J.P. Du, C.Y. Wang, T. Yu, Modell. Simul. Mater. Sci. Eng. 21 (2013) 015007.
[30] J. Rifkin, Center for Simulation, University of Connecticut, CT, 2002. <http://xmd.sourceforge.net/>.
[31] G.C. Sih, H. Liebowitz, Mathematical theories of brittle facture, Fracture: An Advanced Treatise, vol. 2, Academic Press, New York, 1968 (Chapter 2).
[32] Z.G. Liu, C.Y. Wang, T. Yu, Modell. Simul. Mater. Sci. Eng. 21 (2013) 045009.
[33] Y. Zhou, Z.G. Mao, C.B. Morrison, D.N. Seidman, Appl. Phys. Lett. 93 (2008) 171905.
[34] X.Y. Yang, W.Y. Hu, J. Appl. Phys. 115 (2014) 153507.
[35] Y. Mishin, Acta Mater. 52 (2004) 1451–1467.
[36] Y.F. Guo, C.Y. Wang, Comput. Mater. Sci. 40 (2007) 376–381.
[37] P. Lazar, R. Podloucky, Phys. Rev. B 78 (2008) 104114.
[38] J. Riedle, P. Gumbsch, H.F. Fischmeister, Phys. Rev. Lett. 76 (1996) 3594.
[39] P.A. Gordon, T. Neeraj, Acta Mater. 57 (2009) 3091–3100.
[40] F.H. Wang, C.Y. Wang, Phys. Rev. B 57 (1998) 289.
[41] D. Guenzburger, D.E. Ellis, Phys. Rev. B 45 (1992) 285.
[42] D.E. Ellis, G.A. Benesh, E. Byrom, Phys. Rev. B 16 (1977) 3308.
[43] C.Y. Wang, Defect Diffus. Forum 125 (1995) 79–110.